

Pore Characteristics of the Upper Carboniferous Taiyuan Shale in Liaohe Depression

Jian Xiaofei^{1,2*}, Liu Renhe^{2,3,4}, Tang Shuheng¹, Lin Wen³, Zhang Qin^{3,4}, and Jia Lingxiao¹

¹China University of Geosciences, Beijing 100083, China

²National Research and Development (Experimental) Center for Shale Gas, LangFang 065007, China

³Research Institute of Petroleum Exploration and Development-LangFang, LangFang 065007, China

⁴China University of Petroleum, Beijing, 102249, China

ABSTRACT

High pressure mercury, nitrogen adsorption, nano-CT, and scanning electron microscope with energy spectrum analysis were conducted on core shale samples for studying the characteristics of Taiyuan formation in the eastern uplift of Liaohe depression. The research results show that the shale gas reservoir pores are mainly open pores such as the wedge-shape pores and parallel-plate pores. By a genetic type, pores mainly include organic pore, pyrite crystal particle pore, illite intragranular pore, illite-smectite mixed layer intragranular pore, and feldspar dissolved pore. The micropore and mesopore play an important role in shale gas reservoir, and their surface area and pore volume are 9.56 m²/g, 0.0414 mL/g, 97.3%, and 68.8% respectively. The pores diameter presents a bimodal distribution with two main peaks at 43 nm and 6.35 μm. Based on the nano-CT, the porosity is 4.36% and the permeability is 204 nD. The brittle minerals played a supportive and protective role for the pores and controlled their spatial distribution.

Keywords: Liaohe, Marine-continental Transitional Facies, Taiyuan Formation, Shale, Pore

INTRODUCTION

Shale gas refers to the natural gas exploited from organic-rich shale. It is accumulated continuously in shale and is characterized by “self-generation and self-preservation” [1-2]. The successful development of the shale gas in North America proves that it is an important type of alternative clean energy [3,4]. The shale of China is characterized by an old age, multiple phases of tectonic reworking, and high evolution degree compared with that of the North America [1-5]. Previous experts (Liu Honglin et al., 2012; Wang Libo et al., 2013; Pu Boling et

al., 2014) have conducted a detailed study on the hydrocarbon enrichment pattern, reservoir space, adsorption features, and storage conditions of the marine shale gas reservoirs in the Southern China, and significant breakthrough has been acquired [5-7]. The shale gas of Chongqing Fuling was the first to put into commercial development. Moreover, the demonstration area in Southern Sichuan and Northern Guizhou has also made a significant progress [8, 9]. Compared with marine shale, continental shale is characterized by a thin thickness, a low content of brittle minerals, a high

*Corresponding author

Jian Xiaofei

Email: 872411052@qq.com

Tel: +86 152 1096 2528

Fax: +86 152 1096 2528

Article history

Received: August 24, 2015

Received in revised form: December 06, 2015

Accepted: January 23, 2016

Available online: July 22, 2017

content of clay minerals, and a low pressure [10-13]; however, the productivity construction of continental shale gas demonstration areas is still steadily advancing through adopting new technologies such as fracturing by CO₂ [14].

At present, studies on the marine-continental transitional facies shale are poor. There is relatively large controversy about the resources potential of the shale of marine-continental transitional facies since it is characterized by a thin reservoir thickness and abruptly changed lithofacies. According to the US Energy Information Administration (EIA) (2011), the shale of marine-continental transitional facies and continental facies in China has no conditions for forming shale gas reservoirs. Assessment of Ministry of Land and Resources (2012) shows the shale gas resources of marine-continental transitional facies are 8.9 trillion square kilometers more than that of continental facies (7.9 trillion square kilometers); therefore, the study on the marine-continental transitional facies shale in the Eastern Uplift, Liaohe Depression is of an important practical significance.

Currently, the kerogen of the marine shale of North American and Southern China as well as the continental shale of the Ordos Basin is predominantly type I and II [15, 16], and studies on shale with kerogen III are lacking. There are two sets of shale of marine-continental transitional facies present in the Eastern Uplift, Liaohe Depression, which were from Upper Paleozoic Carboniferous Taiyuan Formation and Permian Shanxi Formation respectively. Kerogen type of rocks in Taiyuan and Shanxi Formation is type III; therefore, this study on them is of practical and theoretical significance. At present, the shale gas in the area of interest is still in the exploration phase. Previous experts (Ge Mingna et al., 2012; Mao Junli et al., 2012; Ren

Zhunlin et al., 2013; Yu Peng, 2013) have studied the geochemical features, gas generation capacity, gas-bearing property as well as target area selection and the evaluation of shale gas reservoirs [17-21]; however, the economic production of shale gas needs new technology to transform the reservoirs into “artificial reservoirs” with good porosity and permeability. Therefore, the study on reservoir features is critical for the efficient development of shale gas [3, 22-24].

In order to gain an insight into the marine-continental transitional facies shale with kerogen III and to characterize the shale reservoir, this paper quantifies the pores features of the Upper Carboniferous Taiyuan formation shale. Also, the paper provides a reference for the economic development of the marine-continental transitional facies shale in the future.

EXPERIMENTAL PROCEDURES

Geological Setting

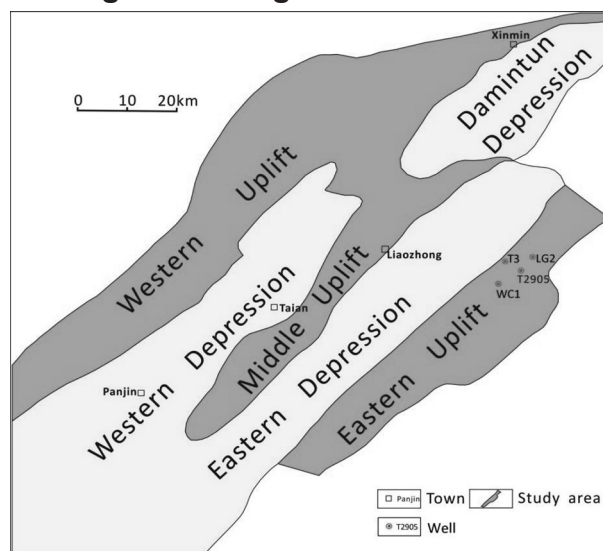


Figure 1: Geological map of eastern uplift in Liaohe depression (according to reference [21]).

Liaohe depression is located in the eastern part of North China plate, adjacent to Liaodong fold belt to the east and Yanshan subsidence zone to the west. It is a Cenozoic rift basin in the central and northern part of the Bohai Bay Basin, with an

area of 1.0×10⁴ km². Liaohe depression presents a tectonic framework of “three uplifts and three sags,” including Western Uplift, Western Sag, Damintun Sag, Central Uplift, Eastern Sag, and Eastern Uplift [19, 21] (Figure 1). The Eastern Uplift is the first-order structural unit in Liaohe depression and is located in the east part, with N-S length of about 80 km, E-W width of about 20 km and an area of 1600 km². Kerogen of Taiyuan formation shale in Liaohe depression is type III and typical humic organic matter, which predominantly generated gas. Its microscopic components were dominated by vitrinite (accounting for 77%), followed by inertinite (accounting for 41%), exinite was the

least. The organic matter of shale had an average TOC of 3% and maturity of 2.1-2.7%. Its Ro value is high, indicating it is in a dry gas phase (Ro> 1.4%). Taiyuan formation of the Upper Carboniferous contains shale, sand, and coal in Liaohe depression. Taiyuan formation shale is the object of this study (Figure 2).

Existing drilling data revealed that the formation thickness of Taiyuan formation was 122.9 to 171.3 m in the Eastern Uplift of Liaohe depression, among which, 48 to 87.4 m was shale interval (Table 1). Eight core samples of shale were all selected from the target shale interval of Taiyuan formation in Well T2905 (Figure 2). Shale samples depth and other related data are in Table 2.

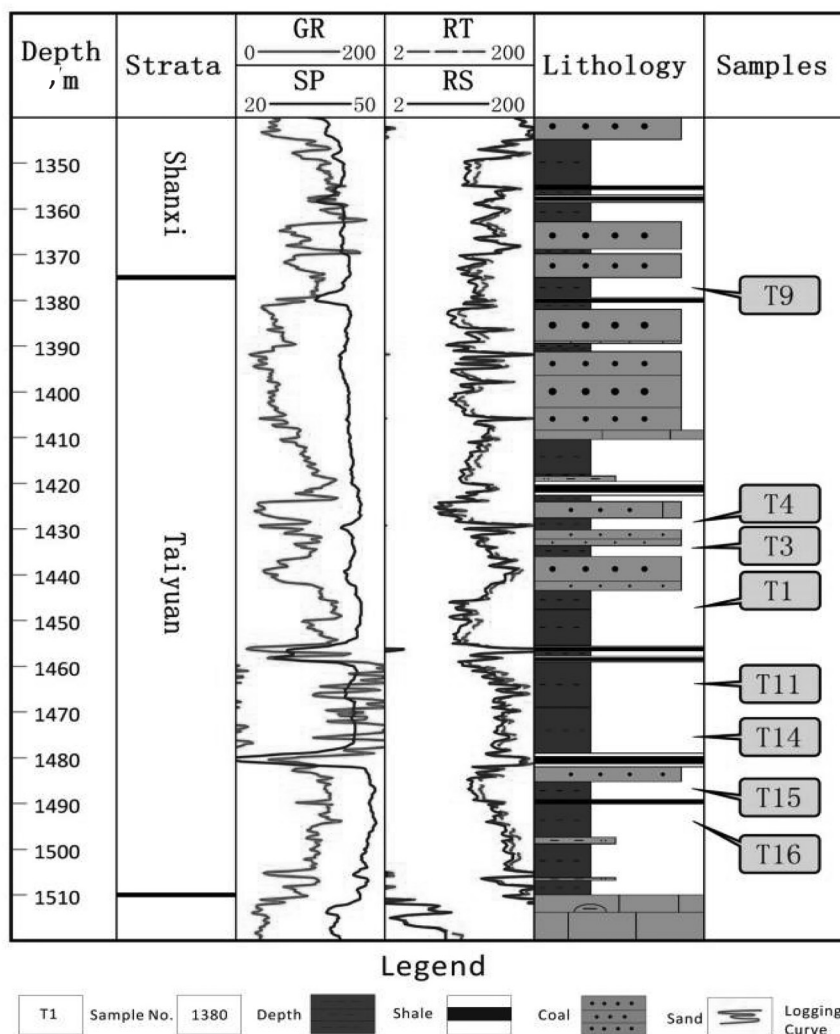


Figure 2: Taiyuan formation comprehensive stratigraphic column.

Table 1: Thickness of Shanxi (P1s) and Taiyuan (C3t) formation in the Upper Carboniferous.

Well	Burial Depth (m)	Total (THK, m)	Shale (THK, m)	Sand (THK, m)	Coal (THK, m)
	P1s/C3t	P1s/C3t	P1s/C3t	P1s/C3t	P1s/C3t
WC1	1754.48/1914.04	159.5/123.1	31.6/60.3	115.2/48.8	12.7/14
LG2	844.5/1015.8	171.4/140	85.3/67.1	77.3/61.1	8.8/11.9
T3	1941.05/2070.95	129.9/122.9	49/87.4	68.5/19.1	12.4/16.4
T2905	1266/1375.06	109/134.8	40.6/48.1	65.4/78.3	3/8.4

Experiments like scanning electron microscopy, CT, nitrogen adsorption, and high pressure mercury injection had obtained some achievements in the characterizing shale pores [25-29], but all of them had their limitations; for example, scanning electron microscopy and CT could not accurately quantify pore features, and nitrogen adsorption method was only limited to characterize the pores with size of 2 to 50 nm; high pressure mercury injection method could not provide adsorption capacity evaluation. In this study, the experiments mentioned above were comprehensively utilized in order to characterize the shale reservoirs of marine-continental transitional facies in the Eastern Uplift of Liaohe depression from multi-scale and multi-view field accurately, qualitatively, and quantitatively. After polished by argon ions, the samples were observed by high-resolution scanning electron microscope, based on which, the pore type, structure, and size were qualitatively analyzed; combined with high pressure mercury injection method and nitrogen adsorption method, the pores with different sizes were quantitatively and accurately characterized. Advanced nano-CT technology had achieved non-destructive test and has been used to exhibit the 3D spatial distribution of the pores, organic matters, and mineral components of shale.

RESULTS AND DISCUSSION

Argon ion polishing, high resolution field emission scanning electron microscopy, energy spectrum

analysis, high pressure mercury injection, nitrogen adsorption, and nano-CT experimental test were performed in order to finely characterize the pore morphology, pore size, pore distribution and porosity, and the permeability of shale reservoirs (Figure 3). The specification of the shale samples for argon ion polishing was 10 mm×10 mm×4 mm. Specific preparation process was as follows: After a small piece of shale sample was knocked off, it was firstly polished using coarse sandpaper; then, it was finely ground using 2000 mesh fine sandpaper in order to make its upper and lower side parallel to each other and vertical to one of its narrow facade. After the sample was processed, its “edge” should be polished by argon ion in order to form a polished triangular surface at the intersection between upper surface and narrow facade. Argon ion polishing experiment was performed by the Key Laboratory of Unconventional Oil and Gas Research Institute of Petroleum Exploration and Development LangFang Branch with the instrument of GATAN693(HAC-200) and gas source of high-purity argon (99.9996%).

After the sample was polished by argon ions, scanning electron microscopy and energy spectrum analysis experiment were performed in Beijing Normal University Testing Center with S-4800(BNUATC-023) field emission scanning electron microscopy and EDAX spectrometer. 8.0 kV voltage was adopted for energy spectrum analysis, whereas, 20.0 kV voltage was adopted for high-resolution scanning electron microscopy analysis. The imaging resolution had reached nanoscale.

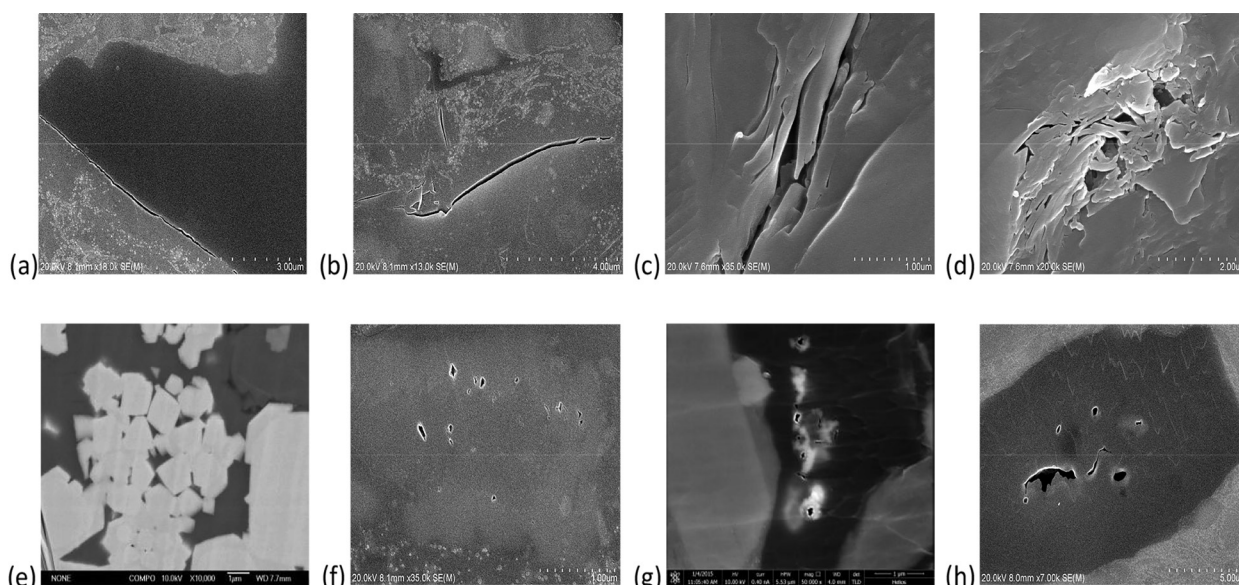


Figure 3: SEM energy spectrum characteristics of minerals and pores in shale samples.
 (a): T15 organic matter and clay mineral marginal fracture; (b): T15 fractures within illite/smectite mixed layer; (c): T9 illite intercrystalline pore; (d): T9 kaolinite intercrystalline pores; (e): T9 pyrite intercrystalline pore; (f): T15 feldspar surfaces dissolved pore; (g): T1 organic matter pore; (h): T16 organic matter pore.

A high pressure mercury injection experiment was performed (Table 2) using AutoPore IV 9520 (YQ-10007) full-automatic mercury injection apparatus with pore size measuring range of 1.8 nm-200 μm, maximum mercury injection pressure of 400 MPa, and mercury injection and ejection volume accuracy of less than

0.1 μL. A high pressure mercury injection experiment was performed by Wuxi Experimental Research Center, Research Institute of Petroleum Exploration and Development, SINOPEC according to the petroleum industry standard SY / T5346-2005.

Table 2: High pressure mercury injection characteristic parameters of Taiyuan formation samples.

Parameters Samples	Burial depth (m)	Brittle minerals (%)	Displacement pressure (MPa)	Maximum connection radius (μm)	Median pressure (MPa)	Median radius (μm)	Residual saturation (%)	Ejection efficiency (%)
T1	1449	55.3	53.25669	0.013801	123.3005	0.005961	45.44427	54.55573
T3	1435.7	56.9	24.07091	0.030535	99.5688	0.007382	45.3444	54.6556
T4	1431.8	59.7	37.79729	0.019446	137.3208	0.005352	38.46313	61.53687
T9	1376.5	51.4	53.27746	0.013796	127.7273	0.005754	31.03269	68.96731
T11	1463.5	55.6	53.26795	0.013798	125.5626	0.005854	31.25196	68.74804
T14	1477.6	62.4	53.26465	0.013799	154.8728	0.004746	22.08751	77.91249
T15	1485.4	55.1	48.06381	0.015292	87.69488	0.008381	42.42424	57.57576
T16	1493.2	47.1	53.28251	0.013794	120.1871	0.006115	32.39362	67.60638
Average	/	55.44	47.04	0.017	122.03	0.0062	36.06	63.94

Nitrogen adsorption specific surface analysis and test were performed (Table 3) after the sample was grinded to 200 meshes or less. The experiment was undertaken by the Key Laboratory of Unconventional Oil and Gas, Research Institute of Petroleum Exploration and Development LangFang Branch. According to the petroleum industry standard SY/T 6154-1995, the test was conducted at a temperature of 120 °C, at a vacuum degree of 1.0×10⁻³ Pa for 5 hrs.

Journal of Petroleum Science and Technology **2017**, 7(3), 67-83
 © 2017 Research Institute of Petroleum Industry (RIPI)

Exploration and Development LangFang Branch. According to the petroleum industry standard SY/T 6154-1995, the test was conducted at a temperature of 120 °C, at a vacuum degree of 1.0×10⁻³ Pa for 5 hrs.

Table 3: Pore size distribution of shale samples tested by N₂ adsorption.

Pore size Samples	Average diameter (nm)	Specific surface (m ² /g)	Pore volume (mL/g)	Pore volume proportion (%)			Specific surface proportion (%)		
				<2nm	2-50nm	50-150nm	<2nm	2-50nm	50-150nm
T1	59.3454	12.5473	0.0527	13.699	55.842	31.206	56.993	44.543	2.746
T3	46.7672	8.5802	0.0466	13.322	58.415	28.325	51.855	46.76	2.529
T4	30.1151	8.1101	0.0311	17.872	66.297	16.052	58.105	41.53	1.445
T9	60.1385	10.7762	0.0474	13.362	57.838	29.561	56.131	45.4	2.79
T11	54.0789	10.7667	0.0463	11.943	60.73	27.791	52.966	47.191	2.689
T14	68.7560	6.5099	0.0394	10.377	61.086	28.609	48.271	49.078	3.091
T15	38.9129	11.1711	0.0428	16.879	62.665	21.244	58.595	43.33	1.885
T16	27.1690	11.2335	0.0425	14.704	59.013	26.294	55.038	43.015	1.964
Average	48.16	9.96	0.0436	14.02	60.24	26.14	54.74	45.11	2.39

Nano-CT scanning experiment was performed (Figure 4) using the nano-CT scanner UltraXRM-L200 produced by Xradia Company. The constant voltage of nano-CT

X-ray source was 40 kV and the photon energy of X-ray was 8 keV. In a high-resolution mode, the viewing area was 15 μm and resolution was 50 nm.

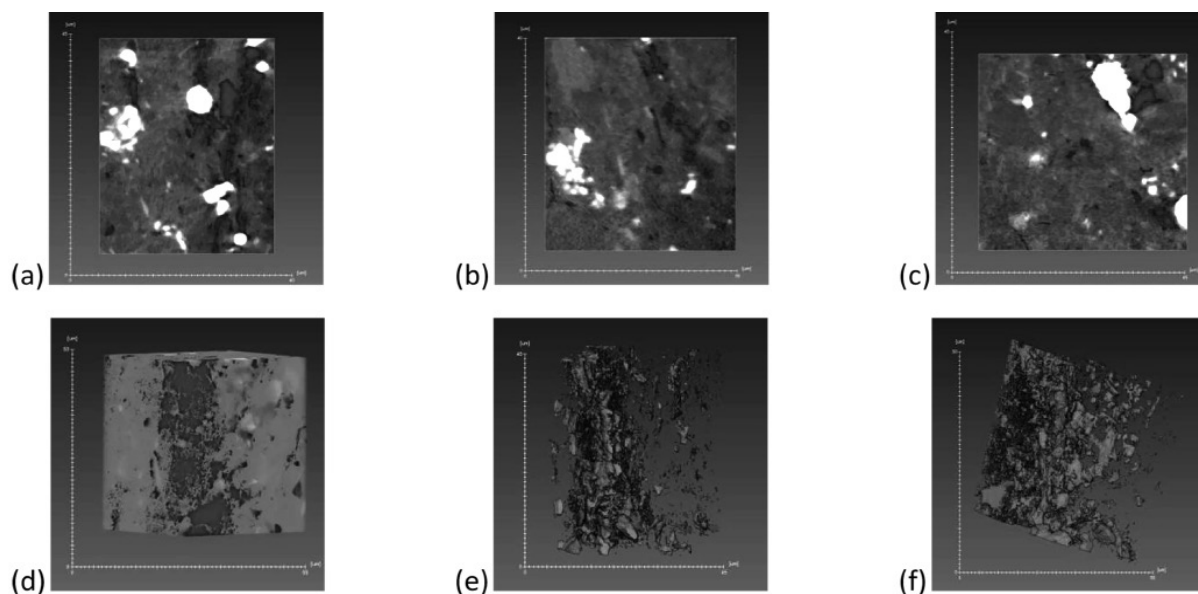


Figure 4: CT images of shale sample T1 from the eastern uplift of Liaohe depression; (a): Cross-section of x-y direction; (b): Cross-section of x-z direction; (c): Cross-section of y-z direction; (d): Segmentation stereographic map; (e), (f): Pore framework.

Pore Morphology

Most pores of shale reservoirs were micron and nano-scaled pores and their development was related to the size of shale reservoir space [4, 30, 31]. Zou Caineng et al. [32] had divided the pores of shale reservoirs into millimeter-scaled (>1 mm),

micron-scaled (1 to 1000 μm), and nano-scaled (<1 μm) according to their sizes. International Union of Pure and Applied Chemistry Association (IUPAC) had divided the micron-scaled pores into macro-pore (> 50 nm), mesopore (2 to 50 nm), and micro-pore (<2 nm) [33].

They also had divided desorption curves into four

types (H1, H2, H3, and H4). The adsorption and desorption branch of H1 were perpendicular to pressure axis and parallel to each other within a wide desorption range, while the adsorption and desorption branch of H4 were horizontal and parallel to each other within a wide pressure range. Samples with the regular pores often presented the loop of type H1, and the samples with micro-pores often presented the loop of type H4; however, the samples with irregular pores often presented the loop of type H2 and H3 [34]. Irregular pores could be divided into open pore (including four-side opened slit-shaped pore and two-side opened cylindrical pore), closed pore (including one-end closed cylindrical pore, parallel plate-like pore and conical pore), and ink bottle pore. Open pore could generate desorption curve, but closed pore could not generate adsorption curve; however, ink bottle pore could generate desorption curve although it was closed at one end. Its desorption curve had a sharply declined inflection point [35].

The nitrogen desorption curves of the experimental

samples (Figure 5) were steep in the vicinity of saturated vapor pressure and gentle around moderate pressure, which was closed to the H3 curve recommended by IUPAC and had the features of H4 curve at the same time. Moreover, the loops exhibited a superposition of a number of standard loops and were a comprehensive reflection of the sample morphology, indicating the pores of the shale gas reservoirs of Shanxi formation and Taiyuan formation in Eastern Uplift Liaohe depression were dominated by the nano-pore with an irregular (amorphous) structure. The studied samples had generated desorption curve, indicating open pores existed in the shale reservoirs of Taiyuan formation (four-side opened slit-shaped pore and two-side opened cylindrical pore); part pores could not generate desorption curve, indicating closed pores existed (one-end closed cylindrical pore, parallel plate-like pore and conical pore); the inflection point of desorption curve was unobvious, indicating ink bottle pores were scarce.

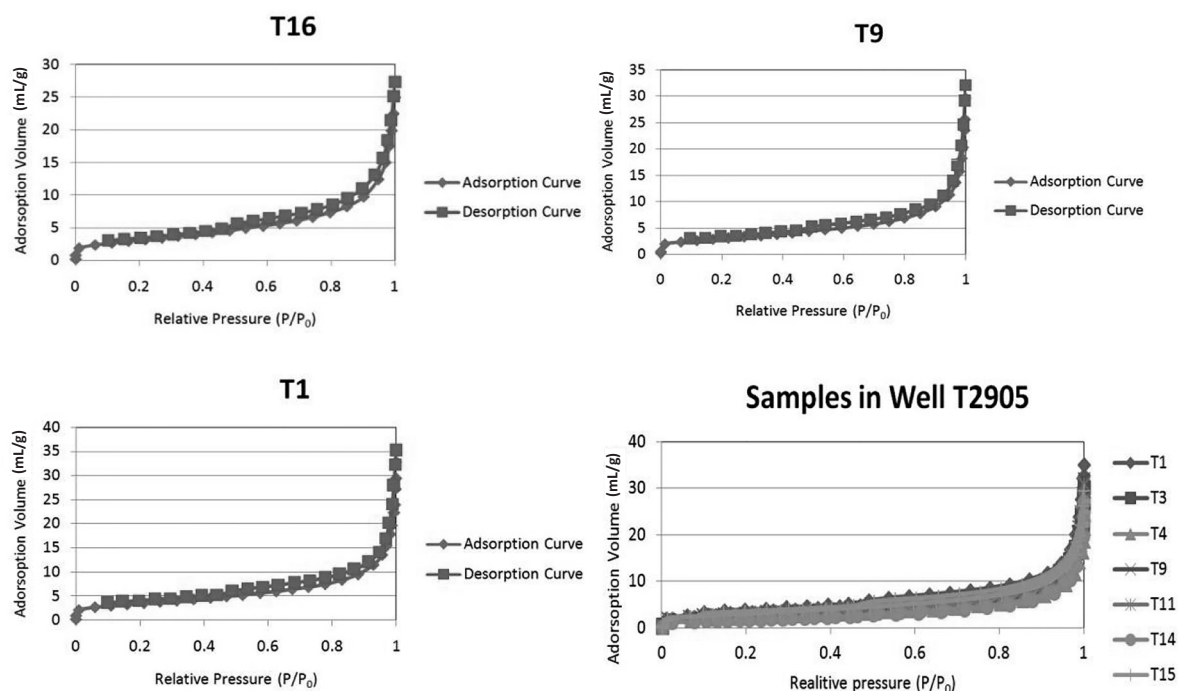


Figure 5: Adsorption isotherms of shale samples from eastern uplift of Liaohe depression.

The measured nitrogen adsorption curves of different experimental samples were typical type II curves, all of which presented an «S» shape. In low-pressure section, the first half of the curve raised slowly and presented a convex shape, indicating the transition stage from adsorbed monolayer into multilayer; in the middle section of the curve, the adsorption amount gradually increased with increasing pressure, indicating a multilayer adsorption stage; in the last half of the curve, the adsorption curve raised sharply; at the end of the curve, adsorption saturation phenomenon did not occur although the

pressure was closed to saturation vapor pressure; this indicates that capillary condensation took place during adsorption process, resulting in the macro-pores filled; therefore, a small amount of meso-pores and macro-pores were existed.

The pore throat of the shale reservoirs of the Eastern Uplift, Liaohe depression was measured by high pressure mercury injection method (Figure 6). The capillary force curve of the shale samples in the area of interest was divided into three sections: initial ascending section, middle gentle section, and end ascending section.

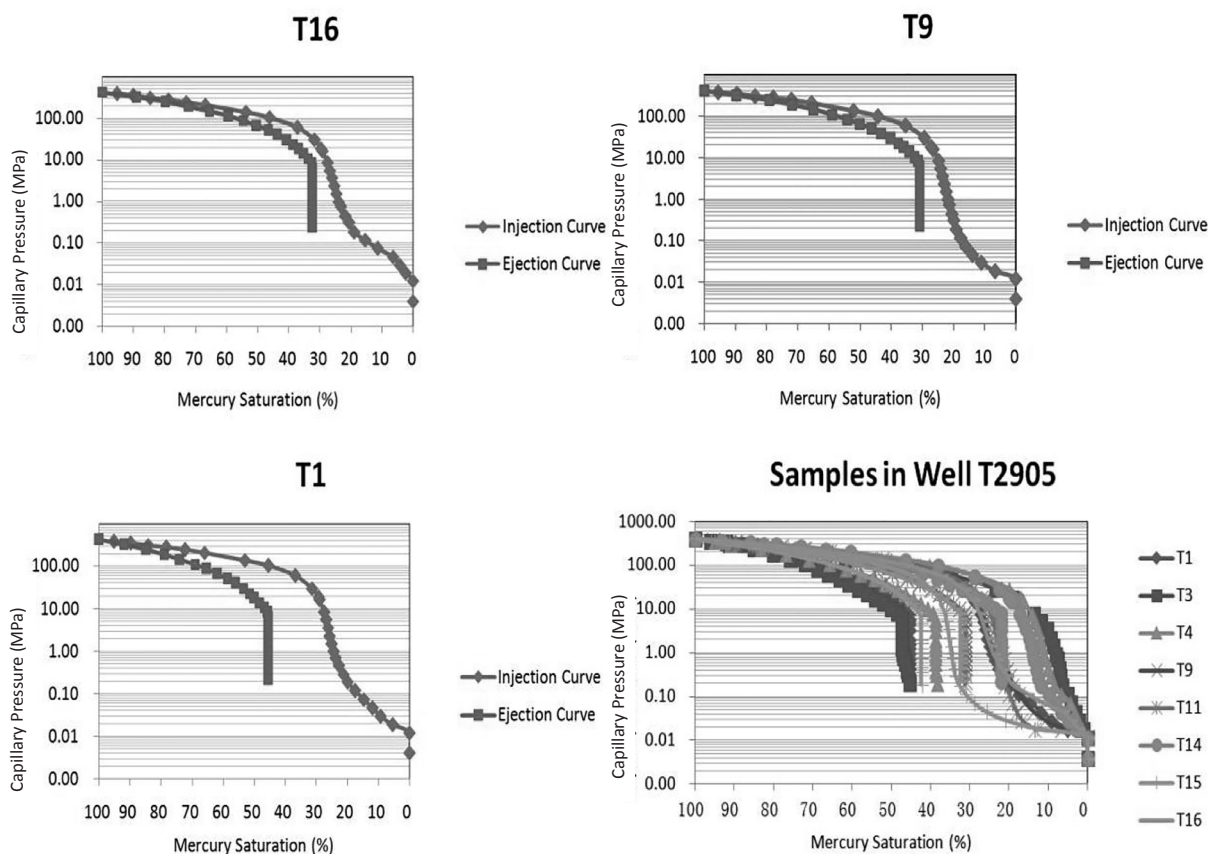


Figure 6: Capillary pressure curve of shale samples from eastern uplift of Liaohe depression.

In initial ascending section, with increasing pressure, mercury saturation increased; non-wetting mercury began to gradually enter into shale, particularly into the pits on shale surface or dissected macro-pore; in the middle gentle section, with further increasing pressure, mercury saturation gradually increased and the number of the macro-pores in shale decreased; at the end of ascending section, with further increasing pressure, mercury saturation increased sharply, indicating mercury began to enter into shale pore in a large amount. The major mercury intrusion section was gentle and long, indicating the pores in the reservoirs were well sorted. The mercury intrusion pressure of the end gentle section ranged between 8 to 378 MPa, indicating the pores with a radius of 2 to 89 nm were extensive in shale. The saturation median radius was between 4.7 to 8.3 nm, with an average of 6.2 nm. The capillary pressure curves were quantitatively studied (Table 2); the results revealed that the averaged displacement pressure of the samples was 47.04 MPa (displacement pressure represented the minimum pressure when mercury started entering into shale, corresponding to the capillary pressure of the largest pore of shale), which was obtained from the intersection point between the extensional line of end ascending section and the y-axis with mercury saturation of 0; this indicates that the maximum connected radius of shale pores was 16.8 nm and the pore connectivity was poor. Moreover, the phenomenon that capillary force curve deviated to upper right, and fine skewness indicated that the pore throat was small in size, and that the pore connectivity was poor. The averaged mercury ejectional efficiency was calculated as 64.85% through residual mercury saturation. The mercury ejectional efficiency was high, indicating most pores were four-side opened slit-shaped pore and two-side opened cylindrical pore, which were advantageous for gas migration.

Pore Type

The micro-pores in shale were semi-quantitatively observed under scanning electron microscope, which were divided into micron-scaled pore and nano-scaled pore. Based on the microscopic components of shale determined from energy spectrum analysis, the pores were divided into micro-fracture, mineral pore, and organic matter pore according to their occurrence.

1) Micro-fracture

Micro-fracture was not apparent in shale, but it was of great significance for the petrophysical property of shale reservoir. It could not only serve as the channel for gas seepage and migration, but also connect micro-pore and macro-fracture, which was of great significance for development [23]. A small amount of micron-scaled micro-fractures were observed in shale, which occurred at the margin of organic matter clumps and minerals (Figure 3-a) or within the clay minerals (Figure 3-b). Organic matter margin fractures occurred at the margin of organic matter and their morphology was related with organic matter clumps. The fractures at the two ends of clay minerals expressed blended saw toothed shape, with a length of about 6 μm , while the fractures within clay minerals were straight and unfilled by minerals, with a length of about 8 μm . The nano-scaled pores and fractures generated by clay minerals had a great contribution to the methane adsorption capacity of shale; this phenomenon was also discovered by other scholars [36, 37].

2) Mineral pore

Matrix pores were extensive in shale in addition to a small amount of micro-fractures. The development of matrix pores was predominately related with the minerals and organic matters in shale, corresponding to mineral pore and organic matter pore. Mineral pore included intergranular pore and intragranular pore. Intergranular pore predominated in shale reservoirs and occurred between the particles of clay minerals

such as illite and kaolinite, and brittle minerals like pyrite. The intergranular pore observed in the shale samples included illite intercrystalline pore (Figure 3-c), kaolinite intercrystalline pore (Figure 3-d), and pyrite intercrystalline pore (Figure 3-e). Intragranular pore included the dissolved pore on feldspar surface (Figure 3-f). Illite intercrystalline pore (Figure 3-c) was located between illite lamella and represented long and narrow tabulate shape. It was formed due the directional arrangement of illite lamella, with a length of 1 to 2 μm and a width of 50 to 300 nm in general.

Kaolinite intercrystalline pores (Figure 3-d) represented two forms; one was the short plate-shaped pore occurred at the margin of kaolinite, part of which had triangular cross-section. It was formed due to the vertical superimposition and arrangement of kaolinite particles, with a width of about 100 nm and a length of no more than 1 μm ; the other was the kaolinite intercrystalline pore that represented "honeycomb". It was formed due to the planner superimposition of hexagonal kaolinite particles. Its diameter was up to 400 nm, representing a good reservoir property.

Pyrite was formed in reducing environment and often associated with organic matter clumps (Figure 3-e) or present in the clay minerals (Figure 3-f). Pyrite crystals generally represented a regular cluster shape, between which an intercrystalline pore was generally formed. Moreover, affected by the crystal shape, the cross section of pyrite intercrystalline pore often exhibited triangular or other polygonal shapes; furthermore, halted by pyrite crystals, the pores were generally unconnected, with a pore size of less than 1 μm .

The dissolved pores on feldspar surface (Figure 3-g) were isolated and scattered and generally exhibited irregular cross section such as circular and ellipse, with a pore size of generally less than 200 nm.

3) Organic matter pore

Organic matter pore was one type of matrix pore. A

large amount of nano-pore was existed within the organic matter particles of shale. Organic matter pore was observed during the study (Figure 3-g and Figure 3-h). Organic matter pore exhibited an irregular shape such as ellipse and was unconnected with each other, with a smooth edge and clear edge sharpness. The pore size of organic matter pore was generally less than 1 μm , with the maximum size of 5 μm . Organic matter pore was closely related with the specific surface area and pore volume of shale and played a positive role in shale adsorbability.

Figure 3 showed that clay mineral pores and pyrite intercrystalline pores were extensive, but organic matter pores were rare, which was resulted from the high content of clay minerals in the samples. The clay mineral content of sample T1, T9, and T15 was 44.7%, 48.6%, and 44.9% respectively, with an average of 46.1% confirming a unimodal distribution in the specific good marine shale reservoir (the clay mineral content of good marine shale reservoir was < 30%). The existing pores shrinkage even disappeared due to the high plasticity of clay minerals, whereas the organic matter pores formed during hydrocarbon generation and expulsion at the late stage was difficult to be preserved since the support and protection of brittle minerals are not present. Similar to the successful development of shale (which also contains high clay minerals more than 40%) in Erdos basin, the shale reservoir of the Eastern Uplift in Liaohe depression still had a development potential.

Pore Size and Distribution

The study results of pore morphology showed that the pores in the shale of Taiyuan formation in the Eastern Uplift, Liaohe depression were dominated by nano-pores, with a certain amount of macro-pore. The pore size and distribution of the nano-pores in shale were characterized from different scales through the combined method of nitrogen adsorption method and

high pressure mercury injection method [38]. According to the results measured by nitrogen adsorption experiments (Table 3), the average pore size of shale was 48.16 nm. BJH pore volume showed that the pore volume of shale reservoir exhibited a bimodal distribution, with two peaks at 2 nm and 100 nm (Figure 7); BET specific surface area showed that the specific surface area of all the samples represented a unimodal distribution, with a peak at 2 nm. Compared with the pores of the marine shale in Southern China surface

area and pore volume, the pores of shale reservoirs in the Eastern Uplift, Liaohe depression expressed a bimodal distribution in pore volume and a unimodal distribution in specific surface area, indicating the polarization of the pores in the shale of marine-continental transitional facies. Meso-pore and macro-pore contributed significantly to pore volume, whereas meso-pore and micro-pore contributed significantly to specific surface area.

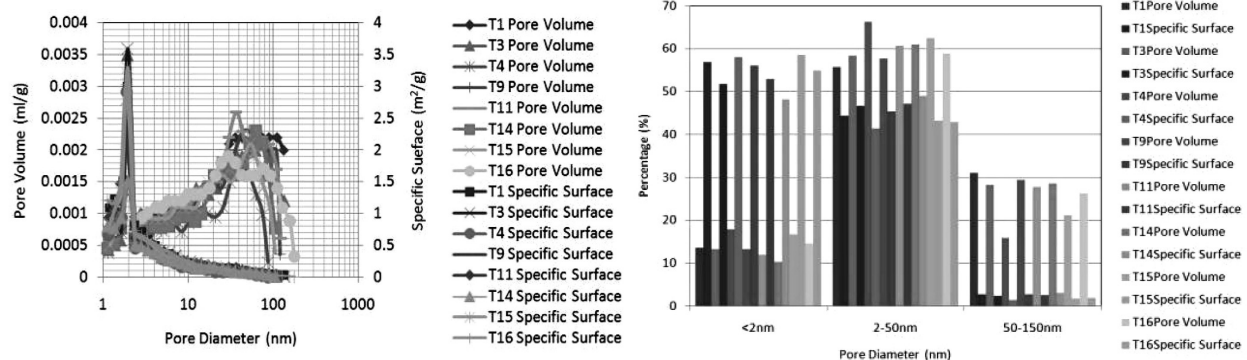


Figure 7: Pore size distribution of shale samples tested by N₂ adsorption.

Quantitative analysis results (Table 3) also revealed a bimodal distribution for pores. The BET specific surface area of shale was 6.37 m²/g to 12.55 m²/g, with an average of 9.56 m²/g; the specific surface area of micro-pore, meso-pore, and macro-pore accounted for 14.6%, 62.4%, and 23.5% respectively, among which the specific surface area of meso-pore and micro-pore accounted for 97.86%. BJH pore volume was 0.0234 mL/g to 0.0527 mL/g, with an average of 0.0414 mL/g. The pore volume of micro-pore, meso-pore, and macro-pore accounted for 14.6%, 62.4%, 23.5% respectively, among which, the pore volume of both meso-pore and macro-pore accounted for 85.4%; therefore, for the pores in the shale reservoir in the Eastern Uplift Liaohe depression, the meso-pore and micro-pore had significantly contributed to the specific surface area, which had provided the primary place for methane adsorption; moreover, the

smaller the pore size was, the stronger the adsorption capacity was (adsorption potential was inversely proportional to pore size); however, meso-pore and macro-pore had significantly contributed to the pore volume, which was also the primary place for the occurrence of free gas.

The distribution of macro-pore was characterized by a high pressure mercury injection experiment since nitrogen adsorption method would create a large testing error for the pores with a size greater than 100 nm. Figure 8 showed the mercury saturation corresponding to different pore sizes, which represented the contribution of different pore sizes on pore volume. High pressure mercury injection results indicated that the peak of the macro-pore size was 6 μm and the pore volume of macro-pore accounted for 48.6%.

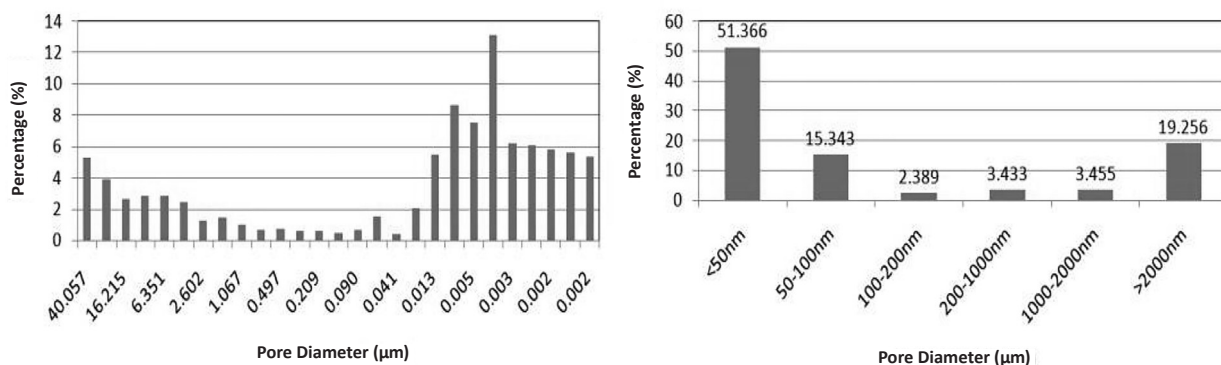


Figure 8: Pore size distribution of shale sample T1 tested by high pressure mercury injection.

Nitrogen adsorption method and high pressure mercury injection method had different measurement results for the pores with different scales. The optimal result segments of each method were selected to be analyzed: for the pores of 2 to 50 nm, the test data of nitrogen adsorption method was selected, while for the macro-pore (> 50 nm), the test data of high-pressure mercury intrusion method was selected. Given that the high pressure mercury intrusion test had a wide applicable range and good macroscopic property, the overall weight of the testing ranges of the two methods were allocated according to the proportion of high pressure mercury injection test (51:49). The comprehensive analysis of the two testing methods is shown in Figure 9. The results of accurate quantitative analysis showed that the two peak values of the bimodal distribution of shale occurred at the point of 43 nm and 6.35 μm respectively.

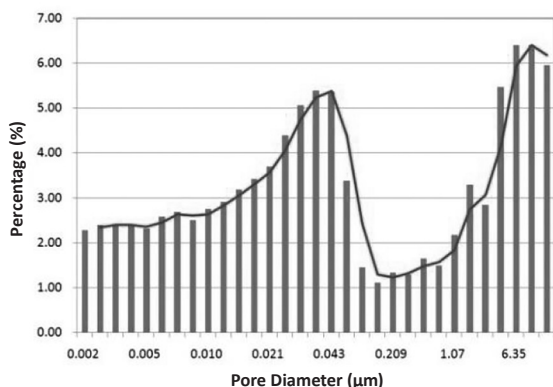


Figure 9: Bimodal distribution of pores in sample T1.

The bimodal distribution and polarization of the micro-pore and macro-pore of shale reservoirs made the pore space have a “clear responsibility” advantage in preserving adsorbed gas and free gas. The two types of pores played different roles in different exploitation phases after fracturing; in the early exploitation phase, free gas predominantly migrated into wellbore and produced productivity, but in late exploitation phase, the adsorbed gas continued desorbing and migrating into meso-pores and macro-pores and provided the major productivity for shale gas. The bimodal distribution of the pores in the shale of marine-continental transitional facies was conducive to the sustainable development of shale gas.

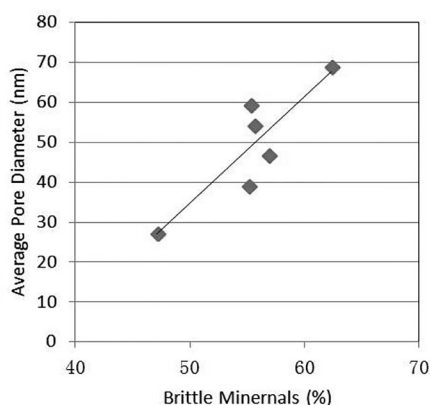
Pore Distribution

CT test was a new technology for charactering pore variation and micro-structure [39]. The pore space distribution of shale reservoir could be quantitatively and semi-quantitatively characterized by CT scanning experiment. The average core porosity measured by CT scanning technology was closed to that measured by He, which exhibited high reliability. The nano-CT experiment of this time obtained 2D and 3D images by taking T1 sample as an example (Figure 4).

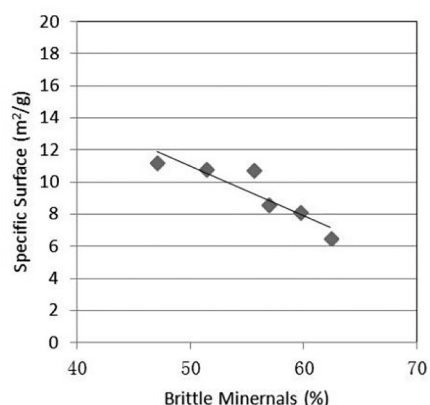
The methane molecules needed the pore throat with a diameter greater than 0.38 nm to migrate since their diameter was only 0.38 nm [40]. The measured CT

shale porosity was 4.36% and permeability was 204 nD; under the conditions that the diameter of shale pores was much larger than that of methane molecules the physical property of shale reservoirs could still meet the conditions for shale gas development. CT scanning images showed different colors for the components with different densities, which could be used to observe the distribution of the different minerals and pores in shale intuitively (Figure 4). Moreover, the brittle minerals such as quartz and feldspar exhibited light color due to high density; clay minerals exhibited gray color due to moderate density; organic matter represented black color due to small density.

After the pores marked blue, it could be found from the thin sections (the blue part in Figures 4a, 4b, 4c), 3D segmentation (the blue part in Figure 4d), and pore stripping framework map (the blue part in Figures 4e and 4f) from different directions that pores represented a continuous and isolated spatial distribution pattern. It could be found from Figure 4a and 4c that the distribution of pores (blue part) and the distribution of brittle minerals were closely related; around the area where brittle minerals were abundant, pores were extensive and continuous; in the area where brittle minerals were scarce, pores were scarce and exhibited an isolated and scattered distribution.



(a) Brittle mineral content and pore size represented positive correlation



(b) Brittle minerals and pore specific surface area represented negative correlation

Figure 10: The relationship between brittle minerals and pores.

Based on the nano-CT qualitative and semi-quantitative analysis, total rock and clay minerals X-ray diffraction experiments were performed in order to analyze the relationship between brittle minerals and pores (Figure 10). Moreover, the results could be used to verify the analysis results of nano-CT experiment. Figure 4a showed that the brittle mineral content was positively correlated with pore size, and that with increasing brittle mineral content, the average pore size increased from 30 nm to 70 nm; Figure 4b showed that the brittle mineral content was negatively correlated

with specific surface area, and with increasing brittle mineral content, the pore specific surface area decreased from 12 m²/g to 6 m²/g. The former revealed the more the brittle minerals were, the larger the pore size was (mostly macro-pore), indicating brittle minerals could support and protect pores; therefore, the pores with a large pore size were formed; the latter revealed that the less the brittle minerals were, the larger the specific surface area was; Table 2 shows that the meso-pore and micro-pore provides 97.86% of the total specific surface area, indicating the

specific surface area had reflected the number of meso-pore and micro-pore; thus, the less the brittle minerals were, the more the meso-pore and micro-pore were; this indicates that the evolved micro-pores even disappear under compaction if they are not supported and protected by brittle minerals. Figure 4a and 4c show that the brittle minerals had a regional distribution (white part), indicating that the pore size also had a regional distribution (macro-pore took dominance around brittle minerals, but micro-pore took dominance in the area where brittle minerals were rare); this verified that the pores in the shale of marine-continental transitional facies had a bimodal distribution from the other side.

The pore spatial distribution of shale was clarified through quantitative-semi-quantitative analysis; the continuous and isolated distribution of pores were mainly controlled by brittle minerals; brittle minerals played a supportive and protective role for pores; where brittle minerals were abundant, pores mostly occurred as large pores with a continuous distribution, but in the area where brittle minerals were not abundant, pores were scarce and mostly occurred as meso-pores and micro-pores with an isolated and scattered distribution.

CONCLUSIONS

Argon ion polishing, scanning electron microscope plus energy spectrum analysis, nitrogen adsorption, high pressure mercury injection, and nano-CT experiments were conducted on the shale reservoirs of marine-continental transitional facies in Taiyuan formation, Eastern Uplift, Liaohe depression, and the following conclusions were achieved:

(1) Most pores were four-side opened slit-shaped pores, two-side opened cylindrical pores, and closed pores, without ink bottle pore in morphology, which included pyrite intercrystalline pore, organic matter

pore, feldspar surface dissolved pore, organic matter and clay mineral marginal pore, illite/smectite mixed layer intragranular tabulate pore, and illite intercrystalline pore.

(2) The BJH pore volume of shale was 0.0234 mL/g to 0.0527 mL/g, with an average of 0.0414 mL/g. Meso-pores and macro-pores were the major occurrence place for free gas, accounting for 85% of the total volume. The BET specific surface area of the shale was 6.37 m²/g to 12.55 m²/g, with an average of 9.56 m²/g. Meso-pores and micro-pores had enhanced the adsorption capacity of the shale, accounting for 97.86% of the total specific surface area. The pore size of shale presented a bimodal distribution, with two peaks distributed at 43 nm and 6.35 μm, which was conducive for the shale gas development.

(3) The shale reservoir had CT porosity of 4.36% and permeability of 204 nD; the pores were continuous and concentrated. Brittle minerals controlled the spatial distribution of the pores in shale and played a supportive and protective role. In the area where brittle minerals were abundant, pores mostly occurred as large pores with a continuous distribution, but in the area where brittle minerals were not abundant, pores were scarce and mostly occurred as meso-pores and micro-pores with an isolated and scattered distribution.

Because of the thin shale and small tight pores in it, many researchers consider that the marine-continental transitional facies shale has no gas potential for development. Also, no company has interest in marine-continental facies transitional shale of Liaohe depression. According to above three conclusions, it is beneficial to produce gas from the shale in Liaohe depression as it has different types; moreover, a bimodal distribution and brittle minerals supported pores.

REFERENCES

- Jinchuan Z., Zhijun J., and Mingsheng Y., "Reservoiring Mechanism of Shale Gas and its Distribution," *Natural Gas Industry*, **2004**, 24(7), 15-18.
- Caineng Z., Zhi Y., Guosheng Z., et al., "Conventional and Unconventional Petroleum "Orderly Accumulation": Concept and Practical Significance," *Petroleum Exploration and Development*, **2014**, 41(1), 14-27.
- Curtis J.B., "Fracture Shale-gas Systems," *AAPG Bulletin*, **2002**, 86(11), 1921-1928.
- Loucks R. G., Reed R. M., Ruppel S. C., et al., "Spectrum of Pore Types and Networks in Mud Rocks and a Descriptive Classification for Matrix-related Mud Rocks Pores," *AAPG Bulletin*, **2012**, 96(6), 1071-1098.
- Honglin L. and Hongyan W., "Adsorptivity and Influential Factors of Marine Shales in South China," *Natural Gas Industry*, **2012**, 32(9), 5-9.
- Libo W., Kai J., Weite Z., et al., "Characteristics of Lower Cambrian Marine Black Shales and Evaluation of Shale gas Prospective Area in Qianbei Area, Upper Yangtze Region," *Acta Petrologica Sinica*, **2013**, 29(9), 3263-3278.
- Boling P., Dazhong D., Songtao W., et al., "Microscopic Space Types of Lower Paleozoic Marine Shale in Southern Sichuan Basin," *Journal of China University of Petroleum (Edition of Natural Science)*, **2014**, 38(4), 19-25.
- Tong-lou G. and Ruo-bing L., "Implications from Marine Gas Exploration Breakthrough in Complicated Structural Area at High Thermal Stage: Taking Longmaxi Formation in Well JY1 as an Example," *Natural Gas Geoscience*, **2013**, 24(4), 643-651.
- Zhigang W., "Breakthrough of Fuling Shale Gas Exploration and Development and its Inspiration," *Oil & Gas Geology*, **2015**, 36(2), 1-6.
- Peng L and Liming J., "Reservoir Characteristics and Potential Evaluation of Continental Shale Gas," *Natural Gas Geoscience*, **2013**, 24(5), 1060-1068.
- Xiangzeng W., Shengli G., and Chao G., "Geological Features of Mesozoic Continental Shale gas in South of Ordos Basin, NW China," *Petroleum Exploration and Development*, **2014**, 41(3), 294-304.
- Guoheng L., Zhilong H, Zhenxue J., et al, "The Characteristics and Reservoir Significance of Lamina in Shale from Yanchang Formation of Ordos Basin," *Natural Gas Geoscience*, **2015**, 26(3), 408-417.
- Wei Y., Guojun C., Chengfu L., et al., "Micropore Characteristics of the Organic Rich Shale in the 7th Member of the Yanchang Formation in the Southeast of Ordos Basin," *Natural Gas Geoscience*, **2015**, 26(3), 418-426.
- Xiangzeng W., Jinqiao W., and Juntao Z., "Application of Fracturing Technology for Terrestrial Shale Gas Reservoirs," *Natural Gas Industry*, **2014**, 34(1), 64-67.
- Xin-jing L., Su-yun H., and Cheng Ke-ming C., "Suggestions from the Development of Fractured Shale Gas in North America," *Petroleum Exploration and Development*, **2007**, 34(4), 392-400.
- Xian-ming X., Zhi-guang S., Yan-ming Z., et al., "Summary of Shale Gas Research in North American and Revelations to Shale Gas Exploration of Lower Paleozoic Strata in China South Area" *Journal of China Coal Society*, **2013**, 38(5), 721-727.
- Ming-na G, Jin-chuan Z., Xiao-guang L., et al., "Gas-bearing Property Analysis on Upper Paleozoic Shale in Eastern Uplift of Liaohe Basin," *Fault-Block Oil Gas Field*, **2012**, 19(6), 722-726 (in Chinese with English abstract).

18. Ming-na G, Jin-chuan Z, Xiao-guang L., and et al., "Evaluation on Neopaleozoic Shale Gas Resource Potential in the Eastern Salient of the Liaohe Depression," *Natural Gas Industry*, **2012**, 32(9), 28-32.
19. Junli M., Xiaoguang L., Yansheng S., et al., "Shale Gas Accumulation Conditions of Eastern Region of Liaohe Depression," *Earth Science Frontiers*, **2012**, 19(5), 348-355.
20. Zhunlin R and Xiaoguang L., "Enrichment Condition of Lishugou Formation Shale Gas and Favorable Area Selection in Eastern Area of Liaohe," *Fault-block Oil & Gas Field*, **2013**, 20(6), 704-708.
21. Peng Y., "Application of Widely-covered Hydrocarbon Generation Concept to Hydrocarbon Accumulation in Eastern Uplift, Liaohe Depression," *Journal of Xi'an Shiyou University (Natural Science Edition)*, **2014**, 29(4), 24-37.
22. Dazhong D., Caineng Z., Jianzhong L., et al., "Resource Potential, Exploration and Development Prospect of Shale Gas in the Whole World," *Geological Bulletin of China*, **2011**, 30(2/3), 324-326.
23. Hongyan W., Yuzhang L., Dazhong D., et al., "Scientific Issues on Effective Development of Marine Shale Gas in Southern China," *Petroleum Exploration and Development*, **2013**, 40(5), 574-579.
24. Caineng Z., Dazhong D., Shejiao W., et al., "Geological Characteristics, Formation Mechanism and Resource Potential of Shale Gas in China," *Petroleum Exploration and Development*, **2010**, 37(6), 641-643.
25. Shujing J., Hui H., Qingping W., et al., "Scanning Electron Microscope Analysis of Porosity in Shale," *Journal of Chinese Electron Microscopy Society*, **2012**, 31(5), 432-436.
26. Gengshe Y. and Hui L., "Study on the Rock Damage Characteristics Based on the Technique of CT Image Processing," *Journal of China Coal Society*, **2007**, 32(5), 463-468.
27. Bin B., Rukai Z., Songtao W., et al, "Multi-scale Method of Nano(Micro)-CT Study on Microscopic Pore Structure of Tight Sandstone of Yanchang Formation, Ordos Basin," *Petroleum Exploration and Development*, **2013**, 40(3), 329-333.
28. Wang Jialu W., Jian G., and Li L., "Porosity Characteristics of Sandstone by X-ray CT Scanning System," *Acta Petrolei Sinica*, **2009**, 30(6), 887-893.
29. Xiaoxia S., Yuegang T., Wei L., et al., "Advanced Characterization of Seepage Pores in Deformed Coals Based on Micro-CT," *Journal of China Coal Society*, **2013**, 38(3), 435-440.
30. Haikuan N., Ruikang B., Peixian Z., et al., "Micro-types and Characteristics of Shale Reservoir of the Lower Paleozoic in Southeast Sichuan Basin, and their Effects on the Gas Content," *Earth Science Frontiers*, **2014**, 21(4), 331-343.
31. Boling P., Dazhong D., Chuang E., et al., "Favorable Reservoir Characteristics of the Longmaxi Shale in the Southern Sichuan Basin and their Influencing Factors," *Natural Gas Industry*, **2013**, 33(12), 41-47.
32. Caineng Z., Rukai Z., Bin B., et al., "First Discovery of Nano-pore Throat in Oil and Gas Reservoir in China and its Scientific Value," *Acta Petrologica Sinica*, **2011**, 27(6), 1857-1864.
33. Rouquerol J., Avnir D., Fairbridge C. W., et al., "Recommendations for the Characterization of Porous Solids," *Pure & Applied Chemistry*, **1994**, 66(8), 1739-1785.
34. Hui L., Shaohua W., Xiumin J., et al., "The

- Configuration Analysis of the Adsorption Isotherm of Nitrogen in Low Temperature with the Lignite Char Produced under Fast Pyrolysis," *Journal of China Coal Society*, **2005**, 30(4), 507-510.
35. Ping C. and Xiuyi T., "The Research on the Adsorption of Nitrogen in Low Temperature and Micro-pore Properties in Coal," *Journal of China Coal Society*, **2001**, 26(5), 552-556.
36. Ross D. J. and Bustin R. M., "Shale Gas Potential of the Lower Jurassic Gordondale Member, Northeastern British Columbia, Canada," *AAPG Bulletin*, **2007**, 55(1), 51-75.
37. Shuheng T. and Erping F., "Methane Adsorption Characteristics of Clay Minerals in Organic-rich Shales," *Journal of China Coal Society*, **2014**, 39(8), 1700-1706.
38. Feng Y., Zhengfu N., Detao K., et al., "Pore Structure of Shales from High Pressure Mercury Injection and Nitrogen Method," *Natural Gas Geoscience*, **2013**, 24(3), 450-455.
39. Jialu W., Jian G., and Li L., "Porosity Characteristics of Sandstone by X-ray CT Scanning System," *Acta Petrolei Sinica*, **2009**, 30(6), 887-893.
40. Nelson P H., "Pore-throat Sizes in Sandstones, Tight Sandstones, and Shales," *AAPG Bulletin*, **2009**, 93(3), 329-340.